

# Quadrant kinoform: an approach to multiplane dynamic three-dimensional holographic trapping

Federico Belloni<sup>1,\*</sup> and Serge Monneret<sup>2</sup>

<sup>1</sup>Centre d'Immunologie Marseille-Luminy, CNRS, Institut National de la Santé et de la Recherche Médicale, Parc Scientifique de Luminy, Case 906, 13009 Marseille, France

<sup>2</sup>Institut Fresnel, Domaine Universitaire de St. Jerome, 13397 Marseille, France

\*Corresponding author: federico.belloni@fresnel.fr

Received 18 December 2006; revised 26 March 2007; accepted 27 March 2007;  
posted 4 April 2007 (Doc. ID 78119); published 6 July 2007

Real-time dynamic holographic optical tweezers suffer from an intrinsic limitation. The diffractive optical element, which is the key to reconstruction, requires time for the calculation and physical constraints to be satisfied. In particular, when working in a volume these requirements become highly expensive. Quadrant kinoform represents an alternative to traditional 3D holograms. A spatial domain multiplexing combined with lens term phase profiles allow the independent addressing and control of different planes in the reconstruction volume. The bidimensional holograms used pose less severe physical constraints and the reduced size leads, at the cost of a lower reconstruction resolution, to a consistent speedup in the computation time thus improving real-time interactions. © 2007 Optical Society of America

*OCIS codes:* 140.7010, 170.4520, 090.1760.

## 1. Introduction

In the past decade, optical tweezers have drawn more and more attention as several works explored the multiple possibilities that this technique can offer [1,2]. However, optical tweezers are still struggling to find a stable place in laboratories as a common tool for assays. This seems to be mainly due to the lack of ability in quickly adapting to assay conditions.

One of the most versatile approaches to trapping is holographic optical tweezers (HOT), which appeared for the first time in 1998 at the University of Chicago [3] and have the peculiar capability of addressing the whole sample volume in its three dimensions and virtually generate any kind of light distribution [4]. HOT are based on the diffraction process of computer calculated diffractive optical elements (DOE), usually phase-only holograms also called kinoforms [5]. However, the holographic approach suffers the handicap of computation time and of physical constraints which, if not fulfilled, would reduce the reconstruction quality [6]. Several works explored the limits of this technique [7,8] and

the algorithms [9–12] at the base of the calculation for DOEs, which are the key to holographic trapping. Earlier assays, mainly based on precalculated sequences of holograms [13], provided nice examples on the capabilities of the holographic approach. Today, as computer power increases and algorithms have been refined, we can actually interactively control 3D patterns in real time [14].

The generalized phase contrast (GPC) is another interesting nonholographic technique to achieve 3D trap patterns in real time [15]. This method relies on the conversion of a phase profile into an amplitude one by means of a phase-contrast filter; therefore there is no calculation at all. Nevertheless, to achieve a 3D trapping the beam profile needs to undergo a spatial polarization modulation that requires another device after the phase modulation step. Subsequently, the beam is split, and the trapping is achieved via two counterpropagating beams focused by two low-numeric-aperture objectives, in order to guarantee a long working distance. This implies differences with the holographic approach: the first one is that the traps mainly rely on the scattering force due to the two beams rather than on the gradient force; this indeed lowers the lateral efficiency of the trapping. Second,

with this approach two traps cannot overlap, i.e., lie on the same vertical axis.

Most of current works concerning multiple real-time 3D trapping of particles rely on holographic trapping and use programmable spatial light modulators. However, the increasing size of the addressable area of such modulators means that, in the near future, it will always be difficult to drive them in real time. As a consequence, alternative approaches based on kinoform sectioning could play an important role [16,17]. Here we propose and demonstrate experimentally the quadrant kinoform (QK) principle that allows an interactive control of trap patterns in three dimensions and time. QK are based on the multiplexing of the kinoform spatial domain combined with lens term phase profiles that allow the independent addressing and control of different planes in the reconstruction volume. The bidimensional holograms used pose less severe physical constraints, and their reduced size leads to a consistent speedup in the computation time thus improving real-time interactions. Great interest in our approach comes from the fact that we use fully discernible addressable subunits in our kinoforms, each one of the subunits addressing a given set of traps: movements of traps from only one of these sets, require only the recomputation of the corresponding single subunit, instead of the entire kinoform as in reference [17]. Moreover, randomly mixing of subunits followed in [17] also leads to additional structures containing high spatial frequencies in the kinoform, which strongly decrease the diffraction efficiency of the kinoform for the actual traps.

This paper is organized as follows. In Section 2, a detailed discussion on holograms requirements and algorithms is reported along with the peculiarities for the 3D case. In Section 3, we present QK, a shortcut for real-time 3D manipulation that overcomes all the mentioned constraints at a reasonable cost. In Section 4, a description of the setup and some preliminary experiments are presented. Section 5 reports a quantitative comparison, based on drag force assays of QK with other trapping techniques. Finally, in Section 6, we draw several conclusions about QK and discuss some future work.

## 2. Holograms Requirements and Used Algorithms

The advent of spatial light modulator (SLM) technology allowed the substitution of static DOEs with computer-generated holograms (CGH), which can be interactively changed in time. SLMs offer an easy and controlled way to modulate light both in amplitude and in phase; nevertheless, SLMs that present best performances in terms of diffraction efficiency and fill factor work in reflection mode, and this fact imposes severe limitations in reconstructing 3D patterns. It has been proved that the system numerical aperture, defined as the amount of the diffracted spectrum that can be recollect and used for the reconstruction (see Fig. 1), is imposed by the physical arrangements of the optics. It is a fundamental parameter to determine the quality of the reconstruction as low values would lead to distortions along the

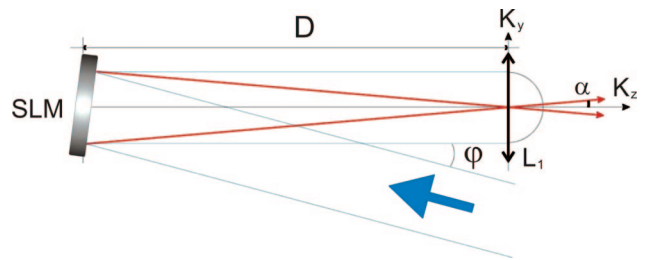


Fig. 1. (Color online) If we consider each point on the SLM as a point source, the system numerical aperture can be defined as  $NA_{\text{system}} = \sin \alpha$  and indicates the restricted set of  $\mathbf{k}$  vectors in the  $\mathbf{k}$  space that are recollect by the first optical element after the SLM, and that can be used for the reconstruction. The angle  $\alpha$  depends on the distance  $D$  of lens  $L_1$  and its aperture. It is clear that working in reflection mode imposes a minimum distance  $D$  to accommodate the lens  $L_1$  in order for it not to obstruct the incoming beam. At the same time, to avoid distortion and lower performances, the angle  $\phi$  formed by the incident and reflected beam on the SLM must be kept as small as possible. Therefore, a trade-off must be made on the  $NA_{\text{system}}$  thus limiting the space of  $\mathbf{k}$  vectors useful for reconstructing the target pattern.

optical axis [6,18]. The use of a beam splitter would allow much higher numerical aperture values but it has not been taken into consideration for the consistent laser power losses it implies (75%). Therefore, optical setup characteristics give the limitation to the axial reconstruction resolution.

A second issue is that previous algorithms based on a trial and error approach cannot be applied anymore in dynamic assays due to the dramatic improvement in SLM technology. Exploring the solution space of a kinoform is not possible anymore because of the increasing resolution and dynamics of modern devices. As an example, let us take a medium-size kinoform of  $512 \times 512$  pixels, each having a phase value comprising between 0 and 255, implying a solutions space of  $\sim 10^{200K}$  possible kinoforms. This huge number can be reduced, and the research carried out on a smaller subset of solutions by using several algorithms in combination. The time required would be in any case far over the real-time threshold we are looking for in dynamic assays. Most of commonly used CGH algorithms rely on the Fourier transform relationship between the DOE plane and the sample plane. They range from combination of gratings and lenses phase distributions to Gerchberg–Saxton (GS) [19] algorithms for 3D light shaping and allow to interactively control a set of optical traps in the volume of the sample [14]. In this paper, we used a conventional GS algorithm with a little tuning on the algorithm parameters to devise our kinoforms. Error-reduction equation coefficients, pseudorandom initialization and integration of the mathematical relationship between the actual phase imposed by the device and the evaluated one, have been implemented to improve the trapping efficiency. The choice of a GS algorithm led us to improve the quality of the reconstructed field at the cost of computation time. This was a fundamental requirement to reach “perfect” kinoforms, allowing us

to compare and evaluate QK performances by minimizing the algorithm dependence.

### 3. Quadrant Kinoform

QK is an approach, partially inspired by the one proposed by Jesacher *et al.* [16] and also followed by Montes-Usategui *et al.* [17], to obtain 3D trapping patterns at reasonable resolutions with an optimized calculation time.

Holograms have the peculiar property to reconstruct the virtual object even when they are broken. Each part of the hologram contains the information about the whole object from different points of view. Therefore, illuminating just a part of it would lead to a full reconstruction of the virtual object but with a lower resolution, good enough, however, to trap particles. Hence, the concept at the base of QK is to multiplex the SLM addressable area into smaller logical units with lower reconstruction efficiency, due to the reduced kinoform size, which are then addressed with a peculiar trap pattern independently. In particular, each unit is devoted to the control of a set of traps on a specific plane. In our case, we limited ourselves to four planes as it provides a good compromise for our assays, hence the name QK. To address multiple planes, each unit is projected onto a different focus depth via the contribution of a coaxial lens term calculated on the base of a defined mathematical expression [see Eq. (1)] where  $n_{med}$  is the medium index;  $\lambda$  is the laser wavelength;  $x$  and  $y$  are the coordinates, the center of the DOE being the origin of the reference system;  $f_{obj}$  is the objective focal length; and  $z$  is the desired focal shift. In such a way, a 3D arrangement of traps can be achieved; the number of units being the addressable planes. The whole procedure can be visualized in Fig. 2. Our approach is in a way similar to the random mask encoding introduced by Montes-Usategui *et al.* [17] but differs by the fact that with each sector we control a specific plane and not a single trap. This enables us to limit the number of sectors to be introduced. The advantage is that our final kinoforms do not present any randomness, i.e., any additional phase distribution with high spatial frequencies that would strongly decrease the global diffraction efficiency of the kinoform by adding extra power dispersion.

$$\phi_{lens}(x, y) = \frac{2\pi n_{med}(x^2 + y^2)z}{f_{obj}^2 \lambda}. \quad (1)$$

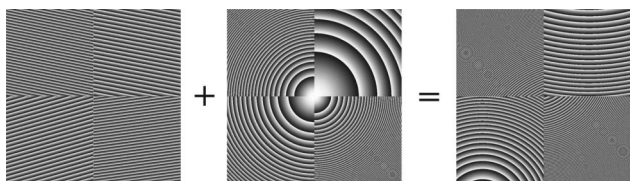


Fig. 2. Basic principle of QK. A hologram composed of four different subunits is combined with four coaxial lens terms to obtain a 3D reconstruction. Here is reported a simple case with only one trap addressed by each subunit.

The main advantage of QK is the reduced computation time. The movement of traps from a given set driven by a given subunit will lead to the recomputation of only the corresponding subunit, which takes roughly a quarter of the time needed for a full kinoform. This because, in our case, each subunit has an area equal to a fourth of the total kinoform. Moreover, the defocusing term takes a calculation time shorter than the refresh rate of the SLM, since it relies on an analytical relation, and can then be considered instantaneous. These two effects combined are enough to achieve an interactive control of the traps, even with the time-consuming GS algorithm chosen in this paper. As a recall, QK does not depend on the algorithm used to generate the kinoforms and will always provide a speedup of the calculation time.

QK also offers advantages also in another typical issue of traditional holograms: the homogeneity of reconstruction defined as the ability to exert the same force in different traps. This should not be confused with the anisotropy of a trap, which is the peculiarity of a single trap to exert different forces in different directions, as discussed later. As a matter of fact, in a multiple trap reconstruction, the strength of each trap is not the same; the common solution consists in evaluating several holograms and preserving the one, which offers the best homogeneity [20] or introducing a slight asymmetry in the trap pattern [21]. Hence, QK exploits the independency of the subunits to increase or reduce their dimensions in order to divert the right amount of light to each reconstruction thus balancing the trap strengths.

The drawbacks of QK are listed below. With QK, we are actually imaging a portion of the SLM active area on a portion of the microscope objective pupil. Therefore, the reconstruction of each subunit will be provided by light coming mainly from certain directions and will form a distorted spot, which in turns gives an anisotropy in the trap strength, i.e., a trap will exert different forces for different directions. This anisotropy does not prevent trapping but must be taken into account when determining the trap stiffness.

### 4. Experimental Setup and Results

The optical setup is built around an inverted microscope and an Hamamatsu X8267-15 programmable phase modulator. The laser beam comes from a near infrared 2W source (IPG Laser, Germany); it is collimated by a first  $8\times$  telescope to overfill the SLM active area in order to have the most possible uniform intensity profile, and finally resized from a second magnification  $<1\times$  telescope to fit the pupil of a  $40\times$ ,  $NA_{objective} = 1.3$  oil oil immersion Zeiss Plan Neofluar objective (see Fig. 3). The sample chamber is a 0.17 mm bottom glass thick (Lab-Tek II, USA) to match the objective specification in order to minimize aberrations due to the high numerical aperture. Additionally, a reference point on the beam path is set to obtain a laser power measure and relate it with the power delivered at the objective pupil. This relationship will give the approximate instant power at the

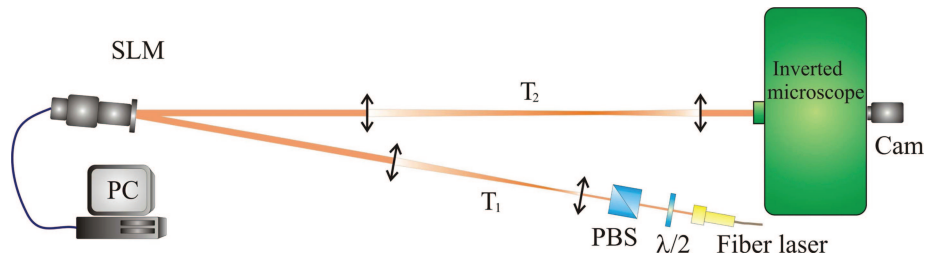


Fig. 3. (Color online) Scheme of the optical bench. The laser beam comes from a near infrared 2W source (IPG Laser, Germany); T1 is a 8 $\times$  telescope to overfill the SLM active area in order to have the most possible uniform intensity profile, while T2 is a magnification <1 $\times$  telescope to fit the pupil of a 40 $\times$ ,  $NA_{\text{objective}} = 1.3$  oil immersion Zeiss Plan Neofluar objective in the inverted microscope. The SLM is an Hamamatsu X8267-15 programmable phase modulator. The  $\lambda/2$  plate is used in combination with a polarizing beam splitter (PBS) to finely adjust the laser power. The PBS is used as well to fix the correct polarization for the SLM.

sample that we will use in our calculations and comparisons of the  $Q$  factors provided that we neglect further reflections from the sample oil–glass–water interfaces; we combine it with the objective transfer function provided by the constructor; and we consider our results on the measured diffraction and collection efficiencies, discussed in Section 5.

To qualitatively check the ability to trap in the QK arrangement, we devised two assays. In the first one, nine silica beads are trapped on three different planes and move at first along the  $z$  axis and subsequently in a peristaltic fashion on the  $xy$  plane (see Fig. 4). The assay is built up on a precalculated sequence of ten kinoforms illuminated by roughly 600 mW at the laser collimator, which gives  $\sim 15$  mW/trap, and takes  $\sim 1$  min in real time. The second clip presents the rotation of four silica beads one over the other, trapped in four different planes at the same time (see Fig. 5). In this case, the sequence is made up of 81 precalculated kinoforms,  $\sim 20$  mW/trap and takes  $\sim 3$  min in real time. A quantitative study of QK is discussed in Section 5.

### 5. Comparison Between Single Tweezers, Single Kinoforms, and Quadrant Kinoforms

In the following paragraphs, we take into consideration three trapping techniques and compare their performances via drag force assays and draw some conclusions about the QK technique. To be able to compare the different techniques, we study the actual power delivered at the sample. As holography relies on a diffraction process, which can lead to power dispersion into higher orders, we must evaluate the impact of this effect on the power collected by the

objective. For this purpose, a simple assay has been devised: for a fixed purpose, a collection of  $\sim 70$  holograms of different kinds (traditional holograms with commonly used patterns, gratings, lens terms, and QKs) has been displayed on the SLM and the collected light that enters the objective pupil measured. In this way, we evaluate the percentage of light lost out of the objective, and that cannot be used for the reconstruction. From the results presented in Fig. 6, we can conclude that the system, in its actual configuration, is able to recollect approximately the 90% of the light we would recollect if no diffraction occurs. It is worth noting that the laser output has an oscillation of 1% about the nominal output. However, nondiffracted light from the zero order also contributes to the measured power in this experiment, with no use for holographic traps. To obtain an estimate of the zero- and higher-orders power losses, we have compared the escape velocity of beads trapped in the same position away from the optical axis: once with a holographic trap, and then with a nonholographic one tilted in order to be in the same position (see Fig. 6). In this way, the two traps have the same optical path, and we can conclude that any difference in performances can be reconducted to the diffraction process. Results showed that for traps inside a circle of radius 10  $\mu\text{m}$  around the zero-order position (see Fig. 6), the holographic trap force, which is directly proportional to the power, can be estimated as only 80% of the nonholographic one. Therefore, the ratio between the power diverted in the first order of an holographic trap and the power of a nonholographic one is 80%. In conclusion, considering both the objective efficiency in recollecting light when diffraction occurs (90%) and the first-order diffraction efficiency (80%), we can expect holographic tweezers

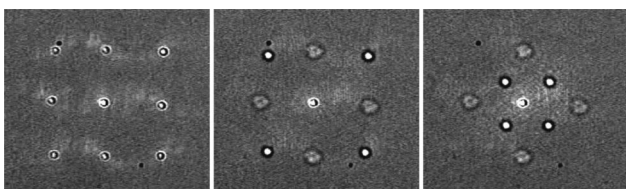


Fig. 4. (3.26 MB) Movie of the first assay of quadrant kinoform reporting nine 2  $\mu\text{m}$  diameter silica beads, which move from a common plane to three different planes and describe a peristaltic movement.

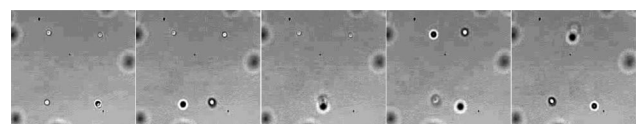


Fig. 5. (2.80 MB) Movie of the second assay of QK showing four 2  $\mu\text{m}$  diameter silica beads, which rotate one over the other each being on a different plane.

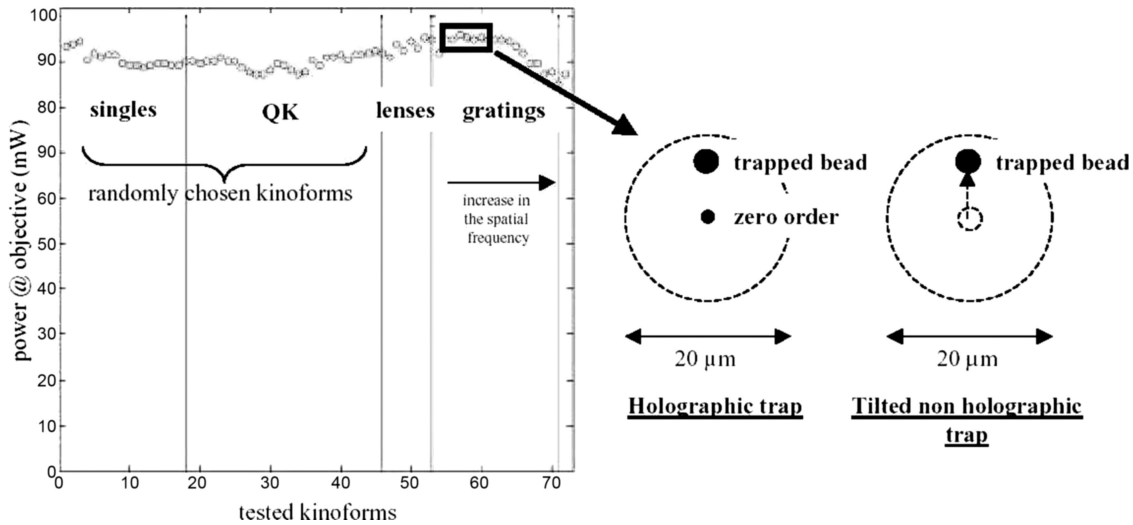


Fig. 6. For a fixed, measured output laser power, several holograms of different kinds (traditional holograms with commonly used patterns, QKs, lens terms, gratings) have been displayed on the SLM and the collected light at the objective pupil measured. Results are shown on the left of the figure. The laser output has an oscillation of 1% around the nominal output. We also estimated the relative trap power for holographic traps and nonholographic ones, for the same trap position, by evaluating the escape velocity of 2.3  $\mu\text{m}$  diameter silica beads (at the right of the figure). For holographic traps, blazed gratings are displayed on the SLM to produce traps relatively close to the beam axis, in order to minimize losses due to light collection by the objective pupil finite area. For nonholographic ones, the SLM is turned off and then acts as a mirror that is mechanically tilted to adjust the trap position. In this way, we are sure that any difference in trap strength is given by the diffraction process and not, for example, by a difference in the optical path or in the focusing away from the beam axis.

to have an optimal strength equal to the 72% ( $0.9 \times 0.8 = 0.72$ ) of the nonholographic ones.

The force of each tweezers type has been derived via the drag force method; a measure of the escape velocity,  $v_{\text{escape}}$ , of a trapped bead (silica 2.3  $\mu\text{m}$  diameter) is used to obtain the trap force via the viscous drag relation  $F_{\text{drag}} = 6 \pi \eta r v_{\text{escape}}$ , where  $\eta$  is the viscosity of the medium [22]. In particular, for the conventional holographic arrangement, we used a pattern of four traps on the corner of a 40  $\mu\text{m}$  side square to prevent cross talk between traps, while in the QK arrangement, the same pattern was employed but with each trap addressed by one of the single-kinoform subunit. Several sets of measures were taken at a distance of 10  $\mu\text{m}$  from the bottom slide. The escape velocities were measured both along the  $x$  and  $y$  axes for each trap. In Fig. 7, we plot the average between the  $x$  and  $y$  measures for each trap and among each peak for the traditional kinoform and QK, moreover for holographic traps the final result is also normalized (multiplication by 4 of the escape velocity) for comparison with the single tweezers. The error bars report the range dispersion of measures around the mean value. From the plot in Fig. 7 and the data reported in Table 1, one of the main drawbacks of traditional kinoforms can be easily visualized: the inhomogeneity of reconstruction, reflected in the bigger error bars of the escape velocity values. This is probably due to aberrations in the optical train that need to be finely corrected. On the other hand, QK is less sensitive to this effect and provides a direct way to counterbalance it by simply modifying the size of each subunit. By doing so, we are able to increase the power delivered to those ho-

lograms that present the weakest reconstruction. However, during the experiments all subunits were kept equal in size.

For a more quantitative analysis of the different techniques, let us consider the quality factor of a trap defined as

$$Q = \frac{F_{\text{trap}} c}{n P_{\text{laser}}}, \quad (2)$$

where  $F_{\text{trap}}$  is the force value recovered from the drag assays,  $c$  is the speed of light,  $n$  is the ratio between the refractive index of the bead and that of the medium, and  $P_{\text{laser}}$  is the laser power at the sample. In such a way, we can directly relate the evaluated value of the force to the trap  $Q$  factor and find that our values of  $\sim 0.03\text{--}0.12$  are comparable with those present in literature [22]. It is worth noting that during the experiments we trapped relatively deep into the sample, at 10  $\mu\text{m}$ , where the efficiency halves due to spherical aberrations [23].

However, the simple kinoform tweezers has a capability of converting light power into force equal to the 51% of the single tweezers ( $Q_{\text{kinoform tweezers}}/Q_{\text{single tweezers}} = 0.060/0.117 = 0.513$ ), while we would have expected the 72%. This difference is probably due to the light diverted into higher orders, because of the 40  $\mu\text{m}$  size of the trap pattern used, which are not all recollected by the objective and thus give rise to additional losses compared with the reference conditions of Fig. 6. In the case of QK, the difference is much more substantial: 31% ( $Q_{\text{QK}}/Q_{\text{single tweezers}} = 0.036/0.117 = 0.308$ ) compared with the expected 72%. This is probably also due to the size of the traps

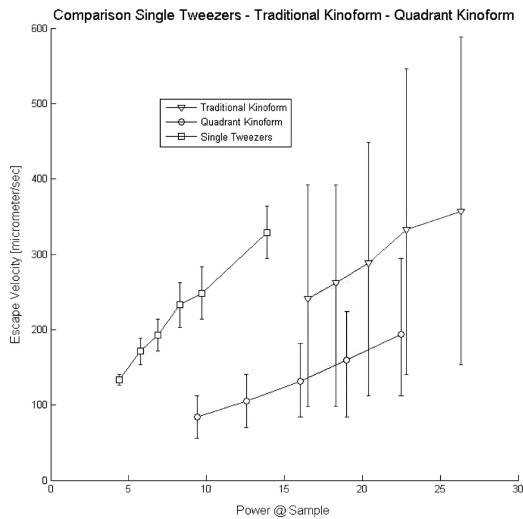


Fig. 7. Forces comparison. The values were recovered from a drag-method assay performed at a distance of  $10\ \mu\text{m}$  from the bottom slide. In the case of the holographic trapping, we employed a four trap pattern on the corner of a  $40\ \mu\text{m}$  side square. In the QK assay, the same pattern was realized addressing each trap with a kinoform subunit. The escape velocities were measured both along the  $x$  and  $y$  axis for each trap. We here plot the average between the  $x$  and  $y$  measures for each trap and among each peak for the traditional kinoform and the QK, moreover for holographic traps the final result is also normalized (multiplication by 4 of the escape velocity) for comparison with the single tweezers. The error bars represent the range dispersion of the measures around the mean value. The bigger error bars in the escape velocity values of the traditional kinoform reflects the inhomogeneity on the reconstruction probably due to aberrations in the optical train. It is important to note how QK is less sensitive to this effect and provides a direct way to counterbalance it by simply modifying the size of each subunit. However, during the experiments all subunits were kept equal in size.

pattern but most of all to the anisotropy in the trap strength due to the previously mentioned spot distortions. A possible solution to traps anisotropies consists in increasing the number of units. We introduce higher spatial frequencies in the hologram and therefore decrease its diffraction efficiency; a trade-off is mandatory. Finally, Table 1 reports the evaluated  $Q$  values and the measured homogeneity for each techniques.

Nevertheless, despite the lower efficiency, QK are still comparable with traditional kinoforms in terms of performances, (their ratio is equal to 0.6), but bring a better homogeneity of reconstruction, a direct way

Table 1.  $Q$  Factors and Inhomogeneity Comparison<sup>a</sup>

	Single Tweezers	Kinoform Tweezers	QK
$Q_{\text{experimental}}$	$0.117 \pm 9\%$	$0.060 \pm 5\%$	$0.036 \pm 5\%$
Inhomogeneity	$0.117\% \pm 9\%$	$\pm 60\%$	$\pm 36\%$

<sup>a</sup>The power used in the calculation of the  $Q$  factor was retrieved by the objective transfer function provided by the constructor. The inhomogeneity is given by the dispersion range from the mean value.

to control it, a faster calculation time, and the possibility to create 3D trap patterns by controlling the focusing depth of each subunit.

## 6. Conclusions and Future Work

We can finally conclude that QK can represent a solid approach to improve real-time 3D optical trapping even when high-quality SLMs and algorithms are used. The fast response time and versatility of the possible patterns should encourage a more consistent development of complex assays for such a technique filling the gap to the moment when we will have highly efficient transmissive SLMs and more powerful, accessible workstations. At present, most of our efforts are directed toward the development of the software interfaces that will provide the necessary user-friendly environment to the nontechnical staff as suggested by Leach *et al.* [14] and Xun *et al.* [24]. At the same time, we are working on the combination of the HOTs setup with microstereolithographic techniques to develop chambers and reservoirs to keep biological specimen and different particles separated [25].

Indeed, a particularly promising domain in biological assays is the regional approach that states how cells are differentiated both in space and time. Therefore, the possibility to investigate such properties provides a solid application for our setup: opsonized particles, e.g., silica or latex beads coated with specific ligands, are put into contact with the target cell in a region-specific and time-resolved manner to explore the variety of responses and subsequently draw a map of cell sensitivity. Several works have pioneered this approach, reporting some encouraging results [26]. However, all of these works were restrained to single or double traps confined on a fixed plane. We intend to extend such an approach to patterns of multiple traps controlled in three dimensions and time via QK.

This work has been supported in part by Carl Zeiss S.A. and the “Conseil Régional de la Région Provence-Alpes-Côte d’Azur.” HOT setup has been supported by the European Funds for Regional Development fundings from the European Commission.

## References

1. D. G. Grier, “A revolution in optical manipulation,” *Nature* **424**, 810–816 (2003).
2. K. C. Neuman and S. M. Block, “Optical trapping,” *Rev. Sci. Instrum.* **75**, 2787–2809 (2004).
3. E. R. Dufresne and D. G. Grier, “Optical tweezer arrays and optical substrates created with diffractive optics,” *Rev. Sci. Instrum.* **69**, 1974–1977 (1998).
4. D. G. Grier and Y. Roichman, “Holographic optical trapping,” *Appl. Opt.* **45**, 880–887 (2006).
5. L. Lesem, P. Hirsch, and J. Jordan, “The kinoform: a new wavefront reconstruction device,” *IBM J. Res. Dev.* **13**, 150–155 (1969).
6. G. Shabtay, “Three-dimensional beam forming and Ewald’s surfaces,” *Opt. Commun.* **226**, 33–37 (2003).
7. M. Polin, K. Ladavac, S. H. Lee, Y. Roichman, and D. G. Grier, “Optimized holographic optical traps,” *Opt. Express* **13**, 5831–5845 (2005).
8. G. Sinclair, P. Jordan, J. Leach, M. J. Padgett, and J. Cooper,

- “Defining the trapping limits of holographical optical tweezers,” *J. Mod. Opt.* **51**, 409–414 (2004).
9. J. E. Curtis, B. A. Koss, and D. G. Grier, “Dynamic holographic optical tweezers,” *Opt. Commun.* **207**, 169–175 (2002).
  10. M. Reicherter, T. Haist, E. U. Wagemann, and H. J. Tiziani, “Optical particle trapping with computer-generated holograms written on a liquid-crystal display,” *Opt. Lett.* **24**, 608–610 (1999).
  11. J. Liesener, M. Reicherter, T. Haist, and H. J. Tiziani, “Multi-functional optical tweezers using computer-generated holograms,” *Opt. Commun.* **185**, 77–82 (2000).
  12. D. Cojoc, V. Emiliani, E. Ferrari, R. Malureanu, S. Cabrini, R. Z. Proietti, and E. Di Fabrizio, “Multiple optical trapping by means of diffractive optical elements,” *Jpn. J. Appl. Phys., Part 1*, **43**, 3910–3915 (2004).
  13. G. Sinclair, P. Jordan, J. Courtial, M. Padgett, J. Cooper, and Z. J. Laczik, “Assembly of 3-dimensional structures using programmable holographic optical tweezers,” *Opt. Express* **12**, 5475–5480 (2004).
  14. J. Leach, K. Wulff, G. Sinclair, P. Jordan, J. Courtial, L. Thomson, G. Gibson, K. Karunwi, J. Cooper, Z. J. Laczik, and M. Padgett, “Interactive approach to optical tweezers control,” *Appl. Opt.* **45**, 897–903 (2006).
  15. P. J. Rodrigo, V. R. Daria, and J. Gluckstad, “Real-time three-dimensional optical micromanipulation of multiple particles and living cells,” *Opt. Lett.* **29**, 2270–2272 (2004).
  16. A. Jesacher, S. Furhapter, S. Bernet, and M. Ritsch-Marte, “Diffractive optical tweezers in the Fresnel regime,” *Opt. Express* **12**, 2243–2250 (2004).
  17. M. Montes-Usategui, E. Pleguezuelos, J. Andilla, and E. Martin-Badosa, “Fast generation of holographic optical tweezers by random mask encoding of Fourier components,” *Opt. Express* **14**, 2101–2107 (2006).
  18. G. Whyte and J. Courtial, “Experimental demonstration of holographic three-dimensional light shaping using a Gerchberg–Saxton algorithm,” *New J. Phys.* **7**, 117 (2005).
  19. R. Gerchberg and W. Saxton, “A practical algorithm for the determination of the phase from image and diffraction plane pictures,” *Optik (Stuttgart)* **35**, 237–246 (1972).
  20. E. R. Dufresne, G. C. Spalding, M. T. Dearing, S. A. Sheets, and D. G. Grier, “Computer-generated holographic optical tweezer arrays,” *Rev. Sci. Instrum.* **72**, 1810–1816 (2001).
  21. J. E. Curtis, C. H. Schmitz, and J. P. Spatz, “Symmetry dependence of holograms for optical trapping,” *Opt. Lett.* **30**, 2086–2088 (2005).
  22. H. Felgner, O. Muller, and M. Schliwa, “Calibration of light forces in optical tweezers,” *Appl. Opt.* **34**, 977–982 (1995).
  23. K. C. Vermeulen, G. J. L. Wuite, G. J. M. Stienen, and C. F. Schmidt, “Optical trap stiffness in the presence and absence of spherical aberrations,” *Appl. Opt.* **45**, 1812–1819 (2006).
  24. X. D. Xun and R. W. Cohn, “Phase calibration of spatially nonuniform spatial light modulators,” *Appl. Opt.* **43**, 6400–6406 (2004).
  25. S. Monneret, F. Belloni, and O. Soppera, “Combining fluidic reservoirs and optical tweezers to control beads/living cells contacts,” *Microfluidics and Nanofluidics* (2007); <http://www.springerlink.com/content/1v21616873485058/?p=665491cc0981482bb0da39d40f2a6651&pi=2>.
  26. X. Wei, B. J. Tromberg, and M. D. Calahan, “Mapping the sensitivity of T cells with an optical trap: polarity and minimal number of receptors for Ca<sup>2+</sup> signaling,” *Proc. Natl. Acad. Sci. U.S.A.* **96**, 8471–8476 (1999).